Available online at www.sciencedirect.com
SCIENCE DIRECT®
Journal of Sound and Vibration 272 (2004) 385–412
JOURNAL OF SOUND AND VIBRATION
www.elsevier.com/locate/jsvi

Detecting damage in beams through digital differentiator filters and continuous wavelet transforms

A. Messina*

Dipartimento di Ingegneria dell'Innovazione, Università degli studi di Lecce, Via Monteroni, 73100 Lecce, Italy

Received 16 September 2002; accepted 20 March 2003

Abstract

Several papers that have recently appeared in the literature have shown the potential offered by certain mathematical tools (wavelets) for detecting damage in systems such as transversally vibrating beams. However, although the applications shown by different authors suggest that the tools show promise, the literature lacks a clear and concise collocation of the wavelets with respect to these previous methods that show similar (if not identical in certain circumstances) performances. In this paper, the continuous wavelet transforms (cwt_s) are discussed and compared, from a theoretical and numerical point of view, with those methods known as differentiator operators. Such differentiator operators adopted as filters are also able (similarly to the cwt_s) to reduce unwanted high frequency noise. Therefore, literature concerning differentiator filters in the digital signal processing area is investigated and several digital filters, known and modified, are analyzed and compared with the cwt_s in the presence of Gaussian noise. The theoretical aspects are discussed in both the non-transformed and Fourier transformed domain. This study results in an attempt to provide an elucidation on the effectiveness and the need to use the considered methods (differentiator filters and/or cwt_s) for detecting damage in transversally vibrating beams.

1. Introduction

Damage detection based on using changes in modal data or in more general vibrational data, has become one of the most attractive research topics in recent years [1–3]. The relevant literature is increasing because of the undoubted advantages offered by these techniques compared with existing diagnostic techniques (acoustic emission, eddy current, radiographic, etc.). The latter can

*Tel.: +39-0832-297-362; fax: +39-0832-325-004.
E-mail address: arcangelo.messina@unile.it (A. Messina).

0022-460X/$ - see front matter © 2003 Elsevier Ltd. All rights reserved.
doi:10.1016/j.jsv.2003.03.009

only detect damage in locations established a priori. However, there are still several unsolved questions. Moreover, a well-established technique has still not been recognized as being suitable for several real cases by researchers and practitioners.

This work is related with those methods that try to detect the existence and location of damage (referred to here as the identification process), by processing the dynamical shapes that are strictly related to the system. This statement leads to the investigation into integrity of a system by avoiding the involvement of a relevant numerical model. The analyst, who should only process a measured signal containing relevant information concerning the damage, has to tackle the identification problem from a clearly better perspective. The so-called 'dynamical shapes' should correspond to a signal defined in the space (mode shapes, dynamic or static deflections, etc.), which is supposed to contain spatial information regarding the identification process. In this study the 'dynamical shapes' will correspond to the mode shapes of certain damaged transversally vibrating beams.

With respect to this particular structural element considered, the first significant attempts could be historically attributed to Yuen [4] and Pandey et al. [5]. These authors reported that derivatives of displacements should be considered as useful tools leading to diagnostic information. Indeed, the numerical simulations carried out by Yuen [4] showed that significant changes can occur in the slopes of displacements in the proximity of the damaged locations. On the other hand, Pandey et al. [5] discovered that a systematic detection of damaged locations in beams could be obtained by looking at certain characteristic peaks associated with the curvature mode shape changes between intact and damaged states. Refs. [4,5] reached such conclusions by using numerical FE-models. A recent numerical investigation conducted by Abdo and Hori [6] also compliments the concept suggested in Ref. [5]. However, the successes obtained by the numerical simulations of Pandey et al. [5] were not always successfully supported by subsequent experimental tests. For example, Chance et al. [7] reported that curvature changes could be masked by the derivative operations in the presence of noisy data. However, other investigators (e.g., Ref. [8]), in other experimental circumstances, found the mode shapes curvature changes to be useful damage detection indicators.

The idea of Pandey et al. [5] was subsequently adopted by Hoerst and Ratcliffe [9] and Ratcliffe and Bagaria [10] who aimed at detecting damaged conditions by avoiding any baseline information of the undamaged structure (a fact generally present in practice). These authors presented a method (*gapped smoothing*), which essentially aimed at extracting certain peaks, characteristic of local damage, by processing the curvature mode shape only in its damaged condition.

The method [9] was also applied to detect open cracks in damaged beams by Gentile and Messina [11] in conjunction with all the derivatives up to the third order. However, the noise still significantly affected the success of the processing techniques mentioned.

Based on all the investigations mentioned previously, there is evidence for stating that the derivatives should be considered useful tools for identifying local damage. However, for the classical derivative operations a careful implementation has to be retained which is important in the presence of noisy data [7,11].

In addition to the derivatives the literature is currently showing a parallel channel of processing techniques through wavelet transforms. As far as the interests of this study are concerned, Refs. [12–14] are of interest. Wang and Deng [12] and Quek et al. [13], investigated the possibility

of identifying the presence and the location of localized damage on transversally vibrating beams by using wavelet analysis. Wang and Deng [12] used a discrete Haar wavelet transform [15,16] to identify the location of damage in beams and plates. Moreover, Quek et al. [13] compared the performances of two different analyzing wavelets: Haar and the complex Gabor wavelets. Hong et al. [14] used the continuous wavelet transform to estimate the damage location and extent by using the Lipschitz exponent [16–18]. The investigation by Hong et al. [14] was based on the '*mexican hat*' wavelet having two vanishing moments. This choice was justified for reasons related to the Lipschitz exponent to quantify the damage extent.

In spite of all the successes mentioned by the previous studies the investigations were conducted without considering a theoretical justification aimed at correlating existing techniques with wavelets. Such a correlation should be considered to be of fundamental importance for supporting the reasons that should lead the investigators to use wavelets rather than derivatives which are more easily applicable and universally known. In this respect, the investigation by Gentile and Messina [19] deserves attention. Indeed, Gentile and Messina pointed out how, to a certain extent, certain continuous wavelet transforms were equivalent to the derivatives when the related dilation parameters approach zero. This equivalence can be identified between the number of vanishing moments and the order of differentiation. Numerical and analytical comparisons showed how the exact correspondence between cwt_s and derivatives operations could effectively occur in practical calculations. However, a substantial difference between cwt_s and differentiators based on finite difference schemes was revealed in the presence of noise. Indeed, Gentile and Messina [19] showed that cwt_s could reduce the noise (amplified through a classical differentiation). The price for this performance is that the lowest scale cannot be considered the best choice to identify the location of the damage, as is usually believed. For this reason, Gentile and Messina [19] pointed out that a trade-off should be adopted to preserve diagnostic details and to reduce the effect of noise through the continuous wavelet transforms when applied on discrete vibrational data.

Ref. [19], however, left some non-negligible questions unsolved, whose elucidation constitutes the main objective of this study. In particular, the *digital signal processing area* (e.g., Refs. [20–22]) suggests the possibility of tackling the differentiation of noisy data through appropriately designed differentiator digital filters. In this respect the literature lacks an appropriate comparison aimed at illustrating whether these digital filters are as effective as the continuous wavelet transform. Therefore, in this study the continuous wavelet transforms are adopted by using fixed scales in order to preserve the comparison with digital differentiator filters and, therefore, the representation through ridges (e.g., Refs. [18,19]), that could reveal the presence of local damage, is not taken into account. At fixed scales, it is shown that Gaussian cwt_s behave in the same way as low-pass differentiator filters. Therefore, in this paper a theoretical presentation of cwt_s and higher order differentiator filters is carried out. The relevant digital filters, which are being dealt with, belong to the class of non-recursive filters. This choice corresponds to the convolution operated through the cwt_s, when applied to discrete data, which can be seen as a non-recursive operation. Numerical and theoretical investigations are conducted in order to identify the reasons that should encourage an analyst to use cwt_s instead of differentiator filters or vice versa. Three different differentiator filters are adopted in this study which belong to a number of technical proposals made over the last 20 years.

2. Theory and applications of digital differentiator non-recursive filters

The theory illustrated here is extracted from the linear variable invariant (LVI) systems theory and is adapted to the subject investigated. The Fourier domain will play a significant role. However, for brevity's sake, the relevant mathematical derivations and related theorems are taken from the specialized literature (e.g., Refs. [21–25]).

2.1. Continuous and discrete signals

Let $y(x)$ be a signal (the dynamical shape) that is defined in its x-physical domain. Eq. (1) gives its representation in the so-called Fourier-domain:

$$Y(\omega) = \mathsf{F}(y(x)) = \int_{-\infty}^{+\infty} y(x)\mathrm{e}^{-\mathrm{i}\omega x}\,\mathrm{d}x, \tag{1}$$

where $Y(\omega)$ is the contribution of each complex eigenvector $\mathrm{e}^{\mathrm{i}\omega x}$ through which $y(x)$ can be re-composed by

$$y(x) = \frac{1}{2\pi}\int_{-\infty}^{+\infty} Y(\omega)\mathrm{e}^{\mathrm{i}\omega x}\,\mathrm{d}\omega. \tag{2}$$

The variable $\omega \in \mathbb{R}$ corresponds to the angular frequency, which has physical dimensions $rad/dim[x]$; $dim[x]$ in this work will correspond to length or samples in the following discrete version. In any case, ω always constitutes the variable in the Fourier-domain.

Eqs. (1,2) are well known as Fourier transform and inverse Fourier transform respectively. A number of important relationships hold for the Fourier transform, the most relevant of which is given in the following equation:

$$\mathsf{F}\left(\frac{\mathrm{d}^m y(x)}{\mathrm{d}x^m}\right) = (\mathrm{i}\omega)^m Y(\omega) = H(\omega)\,Y(\omega). \tag{3}$$

Based on Eq. (3) the differentiator operator can be seen as the application of a high-pass amplifying filter to the signal in the Fourier-domain. Fig. 1 illustrates the amplitude of this ideal filter only for the positive frequencies belonging to [0 1] and with respect to the first four derivatives. Fig. 1 also illustrates corresponding low-pass differentiator filters, which aim at reducing high frequency noise. In this latter respect, it is stressed that any design depends on the intrinsic characteristics of the noise and that here all the following considerations will refer to the case of Gaussian noise whose higher frequencies contributions correspond to unwanted noise.

As is known, the filtering acts in the variable space through the convolution

$$r(x) = \int_{-\infty}^{+\infty} y(z)h(x-z)\,\mathrm{d}z = \int_{-\infty}^{+\infty} h(z)y(x-z)\,\mathrm{d}z = h(x)*y(x) \tag{4}$$

and through a classical product in the Fourier domain (right-hand term of Eq. (3)).

The reduction of unwanted high frequency noise can be obtained by designing a differentiator filter whose frequency response function corresponds to the curve $(\mathrm{i}\omega)^m$ that is constrained to descend with a certain dropout at the cut-off frequency ω_c. This creates a so-called low-pass differentiator filter (Fig. 1) whose numerical performance depends on how much the ideal

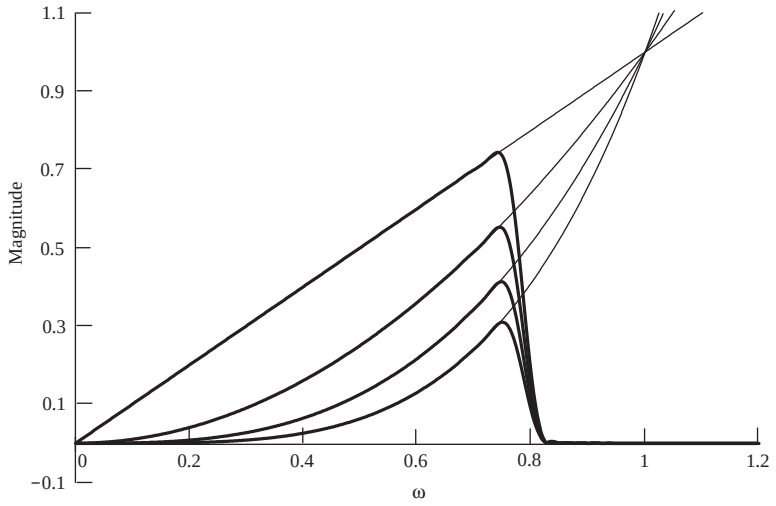

Fig. 1. Differentiator filters $(i\omega)^m$. Ideal (—) and low-pass differentiator filters (——).

filter is approximated from the designed filter as well as on the energy of the signal present in the pass band.

There is substantial discrete technology to believe that a processing technique has to be applied on discrete vibrational data rather than on continuous functions [26]. When the dynamical shape is defined on N discrete values as $y(x_n)$ for $n = 0, \ldots, N-1$, it is still possible to represent such a discrete sequence of numbers in the Fourier-domain. The counterpart of Eqs. (1,2) are Eqs. (5,6) respectively:

$$\bar{Y}(\omega) = \sum_{n=-\infty}^{+\infty} y(x_n) \mathrm{e}^{-\mathrm{i}x_n\omega}, \tag{5}$$

$$y(x_n) = \frac{1}{\omega_s} \int_{-\omega_s/2}^{\omega_s/2} \bar{Y}(\omega) \mathrm{e}^{\mathrm{i}x_n\omega} \, \mathrm{d}\omega, \tag{6}$$

where $\bar{Y}(\omega)$ is a periodic ($\bar{Y}(\omega) = \bar{Y}(\omega + \omega_s)$) Hermitian continuous function defined through real discrete data. The term ω_s corresponds to the sampling frequency and establishes the effective observable frequency band ($[0, \omega_s/2]$ or $[0, \pi]$ if $x_n = n$). It is recalled here that $\bar{Y}(\omega)$ can undergo *aliasing* and is related to the analytical Fourier transform $Y(\omega)$ (Eq. (1)) through the following relationship (for a band-limited signal):

$$\bar{Y}(\omega) = \frac{\omega_s}{2\pi} Y(\omega). \tag{7}$$

Reasonable choices, connected with sampling frequency and the frequency content of the analyzed signals, will be mainly responsible for reducing the aliasing in this study. Moreover, because $\bar{Y}(\omega)$ differs (Eq. (7)) from $Y(\omega)$ by a coefficient $(\omega_s/2\pi)$ it will be indicated as Fourier transform or discrete Fourier transform.

The convolution of discrete signals operated through LVI systems corresponds to the following equation:

$$r(n) = \sum_{n=-\infty}^{+\infty} h(n-k)y(k) = \sum_{n=-\infty}^{+\infty} h(k)y(n-k) = h(n)*y(n). \tag{8}$$

Through Eqs. (5–8) and their related mathematical properties it is possible to realize filters ($h(n)$) that are able to perform the desired operations (low pass differentiator filters in this context) on the numerical sequences $y(n)$.

Finally, since in practice $y(n)$ is constituted by a finite sequence of N numbers and as this study deals with a processing technique through finite impulse response filters (FIR) the summations concerning Eqs. (5,8) have to be adapted over a finite sequence of numbers. Therefore only the N central values resulting from convolution (8) are taken into consideration. This will force the length of the filtered signal ($r(n)$) to coincide with the length of the original signal ($y(n)$).

In the following three sub-sections, Eqs. (5–8) lead to the presentation of the differentiator filters considered in this investigation. The following three FIR-filters were chosen in an attempt to represent chronologically the technical proposals suggested over the last 20 years from the digital signal processing area. They have been considered to be basic in order to show the advantages or disadvantages that can be encountered during their use, at least with respect to an analysis through cwt_s.

It is stressed that in the problem being dealt with, the differentiator filters should be able to conduct a derivation with good accuracy mainly at the lowest frequencies. Indeed, in a generalization dealing with a real signal in the samples domain, the term "frequency" refers to the discrete space (n) where mode shapes are low-frequency signals with respect to the simulated high-frequency Gaussian noise.

2.2. Differentiator filters based on Fourier series method in conjunction with windows (FSW)

This technique can be considered conceptually straightforward as well as being basic in the sense that other methods use part of the same underlying theory. Traces of this method can be found in Refs. [21,22]. The design of the filter starts by assigning the desired frequency response function of the filter ($\bar{H}(\omega)_d$), which, for a low-pass differentiator filter corresponds, in $[-\pi, \pi]$, to

$$\bar{H}(\omega)_d = \begin{cases} (\mathrm{i}\omega)^m & \text{for } |\omega| < \omega_c, \\ 0 & \text{elsewhere.} \end{cases} \tag{9}$$

Due to the periodicity mentioned (Section 2.1), $\bar{H}(\omega)_d$ is expanded in a Fourier series to obtain its related discrete impulse response function $h(n)$. Eq. (10) corresponds to Eq. (6) adapted in the domain $[-\omega_c, \omega_c]$ where the desired frequency response function (10) is different from zero.

$$h(n) = \frac{1}{2\pi} \int_{-\omega_c}^{\omega_c} (\mathrm{i}\omega)^m \mathrm{e}^{\mathrm{i}n\omega} \, \mathrm{d}\omega. \tag{10}$$

The integration of Eq. (10), provides Eqs. (11,12) in a closed non-causal form of the filters for the first two derivatives ($h(n)_m$ refers to the mth derivative). The integrations were also considered for $m = 3, 4$ but for brevity's sake only the first two (11,12) were considered. In accordance with a filter constituted by N_f taps and a sequence n counted from 0 to $N_f - 1$, each occurrence $\widehat{n}$ in the

following equations should be substituted by $n-(N_f-1)/2$. This would result in causal filters for which the central value ($(N_f-1)/2$) would belong or would not belong to the discrete sequence $h(n)$ if N_f is odd or even respectively:

$$h(n)_1 = \begin{cases} \dfrac{\widehat{n\omega_c}\cos(\widehat{n\omega_c}) - \sin(\widehat{n\omega_c})}{\pi\widehat{n^2}} & \text{for } \widehat{n} \neq 0, \\ 0 & \text{for } \widehat{n} = 0, \end{cases} \tag{11}$$

$$h(n)_2 = \begin{cases} -\dfrac{2\widehat{n\omega_c}\cos(\widehat{n\omega_c}) + (\widehat{n^2\omega_c^2} - 2)\sin(\widehat{n\omega_c})}{\pi\widehat{n^3}} & \text{for } \widehat{n} \neq 0, \\ -\omega_c^3/(3\pi) & \text{for } \widehat{n} = 0. \end{cases} \tag{12}$$

Due to the fact that the expansion in Fourier series is based on infinite terms, Eqs. (11,12) should be truncated to obtain a FIR filter. The relevant literature suggests that the truncation should be carried out by weighting the sequence $h(n)$ through an appropriate window $w(n)$ [21,22] in order to face the typical Gibbs phenomenon. In spite of the fact that several windows were used during the simulations, only the case regarding Hamming's window (Eq. (13)) is reported here. This choice is related with the fact that a substantial difference in this application was not revealed by the use of the different windows:

$$w(n) = \begin{cases} 0.54 - 0.46\cos\left(\dfrac{2\pi n}{N_f - 1}\right) & \text{with } 0 \leqslant n \leqslant N_f - 1, \\ 0 & \text{elsewhere.} \end{cases} \tag{13}$$

Fig. 2 shows the magnitude of frequency response functions ($|\bar{H}(\omega)|$) (Eq. (14)) related to the first four derivatives ($m = 1, 2, 3, 4$). The evaluation was made by designing filters, at a fixed cutting frequency ($\omega_c = \pi/2$) with 51 points (N_f). The higher N_f is, the higher the accuracy of the

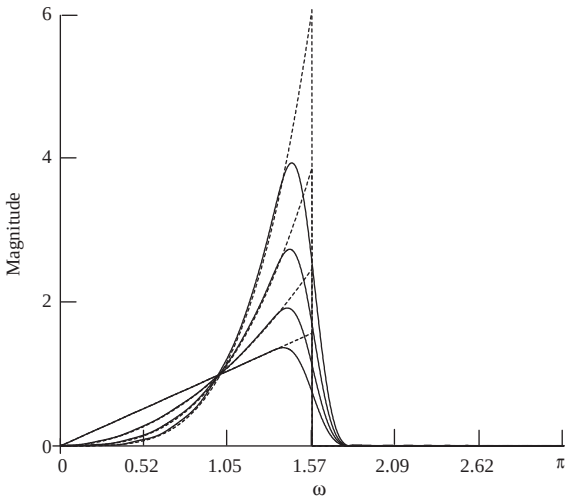

Fig. 2. Desired (- - - $|\bar{H}(\omega)_d|$) and designed (— $|\bar{H}(\omega)|$) differentiator filters for $m = 1, 2, 3, 4$; $\omega_c = \pi/2$, $N_f = 51$. Designs carried out through Fourier series method and based on Hamming window.

designed filter. However, it should take into account that high N_f means long delays and a high loss of data at the ends. Therefore, in the application, the minimum number of taps (N_f) should be preferred:

$$\bar{H}(\omega)_m = \sum_{n=0}^{N_f-1} h(n)_m w(n) \mathrm{e}^{-\mathrm{i}n\omega}. \tag{14}$$

Fig. 2 seems to illustrate a good approximation of the respective ideal filters. However, a perusal of Fig. 2 reveals inaccurate behaviour of the designed filter at the lowest frequencies (these are the main concern in the present application). Such behaviour is revealed by Fig. 3 that displays the logarithmic quantities of Fig. 2 in the observable frequency band $[0, \pi]$, for a different number of points ($N_f = 128, 1024$) and for one cutting frequency (0.15π). For a better visual inspection each pair of curves (i.e., desired and designed filter) has been shifted downward by an amount equal to $m-1$. The higher the slope of curves is, the higher is the correspondent order of differentiation.

The inaccuracy mentioned is not generally observed for the filter concerning the first derivative. Indeed, good accuracy can be observed independently from the cutting frequency and number of points. Conversely, the higher order filters have a certain influence at lowest frequencies and this increases with order of differentiation and does not disappear even for a high number of points (1024). Fig. 3 would suggest cascading the first derivative to obtain a higher differentiation order; however, this practice should only be applied whilst being aware that the length of the filter (i.e., $h(n)_2 = h(n)_1 * h(n)_1$) is approximately doubled. Moreover, the practice of cascading first order differentiator filters does not generally eliminate all the inaccuracies when low values of cutting frequencies are used, as was numerically verified.

Figs. 4 and 5 illustrate the second derivative of the sequence $y(n) = \sin(\pi n/(N-1))$ through two different designed filters. In these figures both the lower graphs illustrate the characteristics of the designed filters and the relevant ideal ones. Figs. 4(c) and 5(c) also illustrate a normalized

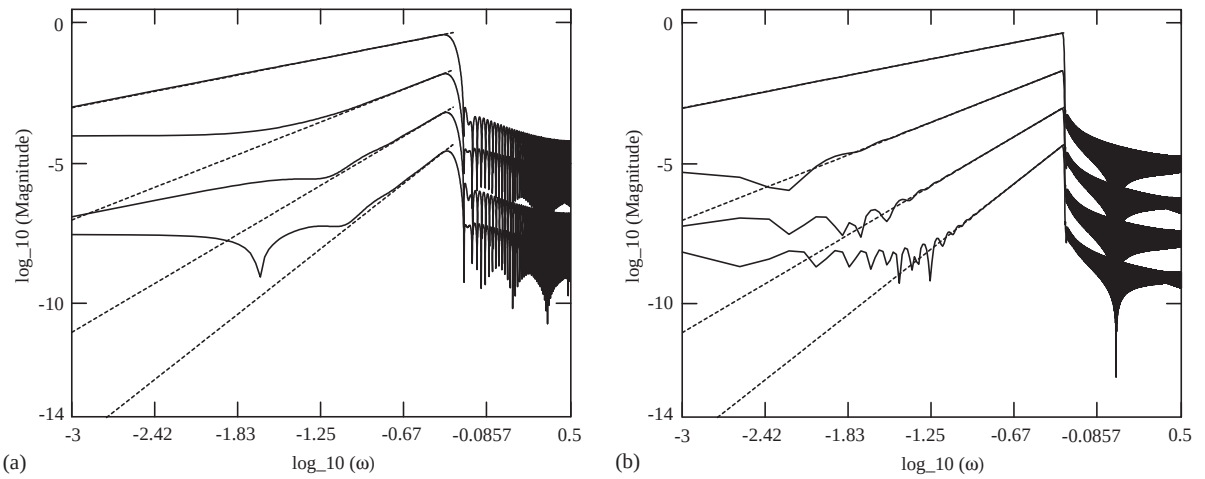

Fig. 3. Log-analysis of non-recursive differentiator filters designed through Fourier series method with $\omega_c = 0.15\pi$ and (a) $N_f = 128$, (b) $N_f = 1024$. ($m = 1, 2, 3, 4$; - - - ideal; — designed.)

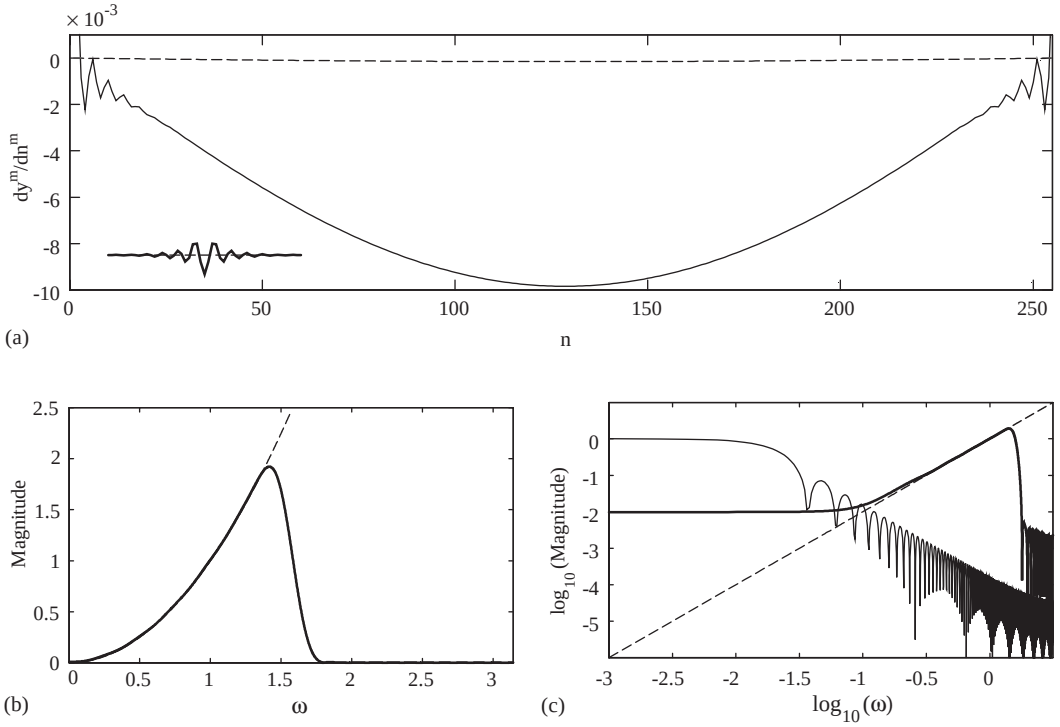

Fig. 4. Second derivative of the signal $y(n) = \sin(\pi n/(N-1))$ ($N = 256$) through a filter $h(n)_2$ designed by Fourier series method and Hamming window with $\omega_c = \pi/2$ and $N_f = 51$. (a) (- - - - exact second derivative); (b) (— $|\bar{H}(\omega)_2|$, - - - ideal differentiator); (c) (— $|\bar{Y}(\omega)|/|\bar{Y}(\omega)|_{max}$, —— $|\bar{H}(\omega)_2|$, - - - ideal differentiator).

Fourier transform of the analyzed signal ($|\overline{Y(\omega)}|/|\overline{Y(\omega)}|_{max}$). This latter graph is used to provide evidence of the frequency content of the signal and assists the interpretation of the simulations. The graphs on the top (Figs. 4(a) and 5(a)) compare the exact second derivative with the filtered numerical one and also show the convolving filter. These filters have length N_f in scale with the abscissa of the leading graph whilst the magnitude does not respect any scale. This arrangement will be considered in all the subsequent graphs.

The filter adopted in Fig. 4 is particularly inaccurate at lowest frequencies. On the other hand, the main frequency content of the analyzed signal (Fig. 4(c)) is mainly located in the frequency range where the filter is inaccurate. This is not clearly shown by the linear representation of Fig. 4(b) that is too optimistic to judge the quality of the filter. As a result, the performance of the numerical derivative results is unacceptable. Conversely, Fig. 5 illustrates a filter whose behaviour is much better than that of Fig. 4. The designs, carried out using the present method, did not follow an immediate methodic way, rather they followed a heuristic process. Such a heuristic method was also supported by checking the accuracy of the filter in the pass-band of interest. Those aspects should be considered to be clear disadvantages with respect to a method that could offer a methodic design of the filter.

With respect to the accuracy of the numerical derivatives, there are reasons to raise the question if the present context requires such high accuracy. Indeed, the context being dealt with regards the

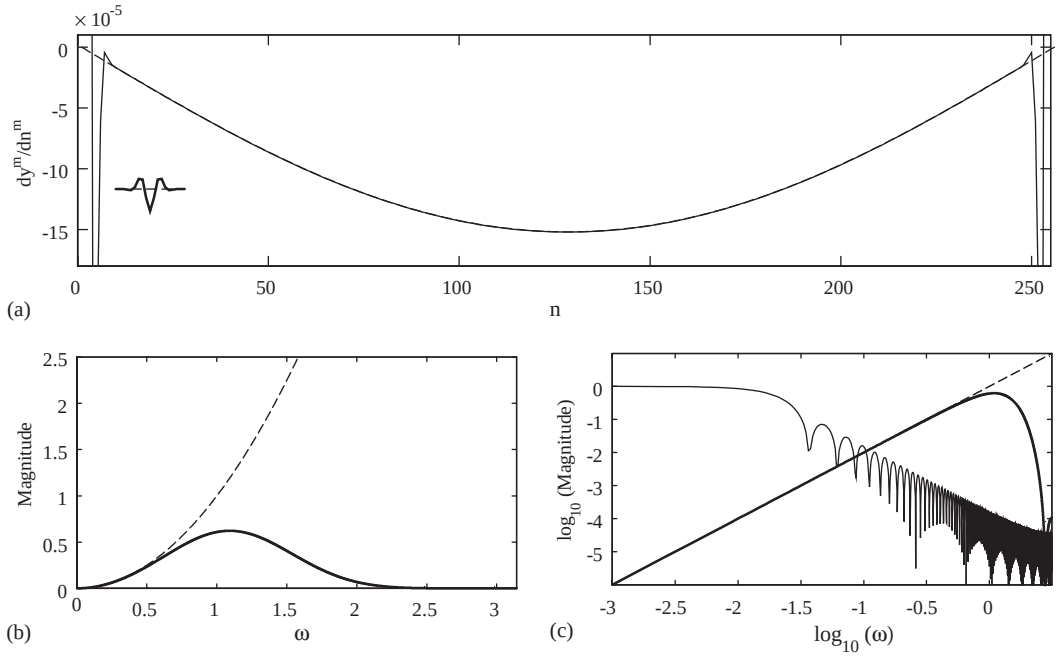

Fig. 5. Second derivative of the signal $y(n) = \sin(\pi n/(N-1))$ ($N = 256$) through a filter $h(n)_2$ obtained by cascading two $h(n)_1$ filters designed by Fourier series method and Hamming window with $\omega_c = \pi/2$ and $N_f = 19$. Keys (a, b, c) referred to Fig. 4.

possibility of detecting damage through a peak in differentiated dynamical shapes. The accuracy could, therefore, be considered as being marginal for an analyst who is only interested in looking for abnormal peaks located on a smooth function. However, a few tests (not reported here for brevity's sake) showed that the inaccuracy could sometimes overestimate the smooth part of the signal and underestimate those peaks that should be preserved as the most interesting part of the signal. Therefore, the accuracy involved in a differentiator filter should also be generally preferred in this context.

2.3. *Differentiator filters based on a weighted least squares technique (WLS)*

The present technique (WLS) has been identified in open literature as an attempt to reduce the problems occurring at the lowest frequencies with filters designed through the FSW method. Other design techniques were identified. However, the WLS technique was retained as the most suitable method in the context.

In particular, Rahenkamp and Kumar [27] present what is possibly the first systematic attempt to design higher order differentiating FIR filters. Their work was based on carrying out modifications to McClellan et al. [28] FIR filter design Fortran program to extend its capabilities to approximate higher order differentiating FIR filters. Subsequently, Pei and Shyu [29] reported that such a proposed method often led to very large deviations or failed to converge. Pei and Shyu [29] proposed a design technique (eigenfilter approach) based on computing an eigenvector

resulting from the constraint imposed on the desired amplitude response. The constraint consists of imposing the response of a designed filter to coincide with its related ideal response at an established arbitrary frequency. Later, Pei and Shyu [30] also developed relevant analytic closed form solutions. It is also of interest to mention Refs. [31,32]. These methods are accurate around the frequency where magnitude and derivative constraints are imposed. A method which tries to globally approximate the ideal filter in the frequency range of interest was proposed by Sunder and Ramachandran [33]. The comparisons carried out by Sunder and Ramachandran showed an accuracy which was comparable to the eigenfilter method [29] without needing to fix an arbitrary frequency to establish the accuracy of the filter. Indeed, the method consists of minimizing the squared error between the ideal response filter and the designed filter over the frequency range of interest. Mollova [34] and Mollova and Unbehauen [35] have also proposed closed analytical formulations for least squares design of digital differentiators.

The previous methods were mainly concerned with full band or *quasi*-full band differentiator filters. As far as the interests of this study are concerned, Sunder and Ramachandran [33, Section VII] discussed an extension of their design technique to other types of frequency selective filters. It is the extension suggested by Sunder and Ramachandran that has been adopted in this work. A slight modification to the extension suggested by Sunder and Ramachandran has been used to tackle problems with the FSW method at lowest frequencies. The following description only concerns the case of even order differentiations through filters with an odd number of points. The remaining three cases were also developed. However, for brevity's sake they were not reported here.

For a non-recursive even order (m) differentiator filter the impulse response function $h(n)$ is symmetric with respect to its centre [22]. Therefore, starting from a non-causal representation, the complex expression (15) can be easily handled to obtain its relevant equivalent form (16):

$$\bar{H}(\omega)_m = \sum_{n=-(N-1)/2}^{(N-1)/2} h(n)_m \mathrm{e}^{-\mathrm{i}n\omega}, \tag{15}$$

$$\bar{H}(\omega)_m = \sum_{n=0}^{(N-1)/2} a(n)\cos(n\omega), \tag{16}$$

where the taps of the filters ($h(n)$) are related to the coefficients $a(n)$ of Eq. (16) by simple relations: $a(n) = 2h(n)$ for $n \neq 0$ and $a(0) = h(0)$. The desired differentiator filter in the frequency domain is illustrated in Eq. (9). Based on Eqs. (9,16) the design technique consists of determining the coefficients $a(n)$ that minimize the following error function:

$$E(a) = \alpha_1 \int_0^{\omega_1} ((-1)^{m/2}\omega^m - \bar{H}(\omega)_m)^2 \,\mathrm{d}\omega + \alpha_2 \int_{\omega_1}^{\omega_c} ((-1)^{m/2}\omega^m - \bar{H}(\omega)_m)^2 \,\mathrm{d}\omega + \beta \int_{\omega_c}^{\pi} ((-1)^{m/2}\omega^m - \bar{H}(\omega)_m)^2 \,\mathrm{d}\omega, \tag{17}$$

where the coefficients $(\alpha_1, \alpha_2, \beta)$ are the weights of the bands delimited by $(0, \omega_1, \omega_c, \pi)$. In total, Eq. (17) is based on three bands: the pass-bands $[0, \omega_1]$, $[\omega_1, \omega_c]$ and the stop-band $[\omega_c, \pi]$. Eq. (17) contains, compared to the suggestion given by Sunder and Ramachandran [33], an additional degree of freedom that is the additional weight in the band $[0, \omega_1]$. This slight modification was

adopted for two reasons: (i) for tackling the inaccuracy that a global method (as it was also the FSW method) undergoes at lowest frequencies; (ii) this is a generalization containing the suggestion of Sunder and Ramachandran [33], which can be obtained simply by settling $\alpha_1 = \alpha_2 = \alpha$.

Therefore, by settling the partial derivatives of the error function to zero ($\partial E/\partial a(n) = 0$), the coefficients $a(n)$ can be obtained by solving the following system of linear equations.

$$\left[\alpha_1 \int_0^{\omega_1} \mathbf{c}\cdot\mathbf{c}^{\mathrm{T}}\,\mathrm{d}\omega + \alpha_2 \int_{\omega_1}^{\omega_c} \mathbf{c}\cdot\mathbf{c}^{\mathrm{T}}\,\mathrm{d}\omega + \beta \int_{\omega_c}^{\pi} \mathbf{c}\cdot\mathbf{c}^{\mathrm{T}}\,\mathrm{d}\omega\right]\cdot\mathbf{a} = \left(\alpha_1 \int_0^{\omega_1} (-1)^{m/2}\omega^m\mathbf{c}\,\mathrm{d}\omega + \alpha_2 \int_{\omega_1}^{\omega_c} (-1)^{m/2}\omega^m\mathbf{c}\,\mathrm{d}\omega\right), \tag{18}$$

where $\mathbf{c}^{\mathrm{T}} = (1, \cos(\omega), \cos(2\omega), \ldots, \cos((N-1)\omega/2))$ and $\mathbf{a}^{\mathrm{T}} = (a_0, a_1, a_2, \ldots, a_{(N-1)/2})$. Once m has been fixed, the elements of Eqs. (18) can be expressed through analytical closed forms and it only remains to solve a system of linear equations.

Fig. 6 illustrates, similar to Figs. 4 and 5, the design of a filter that is able to perform the second derivative of the discrete signal already mentioned using only 9 points. Similar trials were carried out with the FSW method but the design of a filter having a similar short length and a comparable accuracy was unsuccessful. In any case, it is stressed here that the designs were, also in this method, carried out on a heuristic base that was further aggravated by the choice of several parameters.

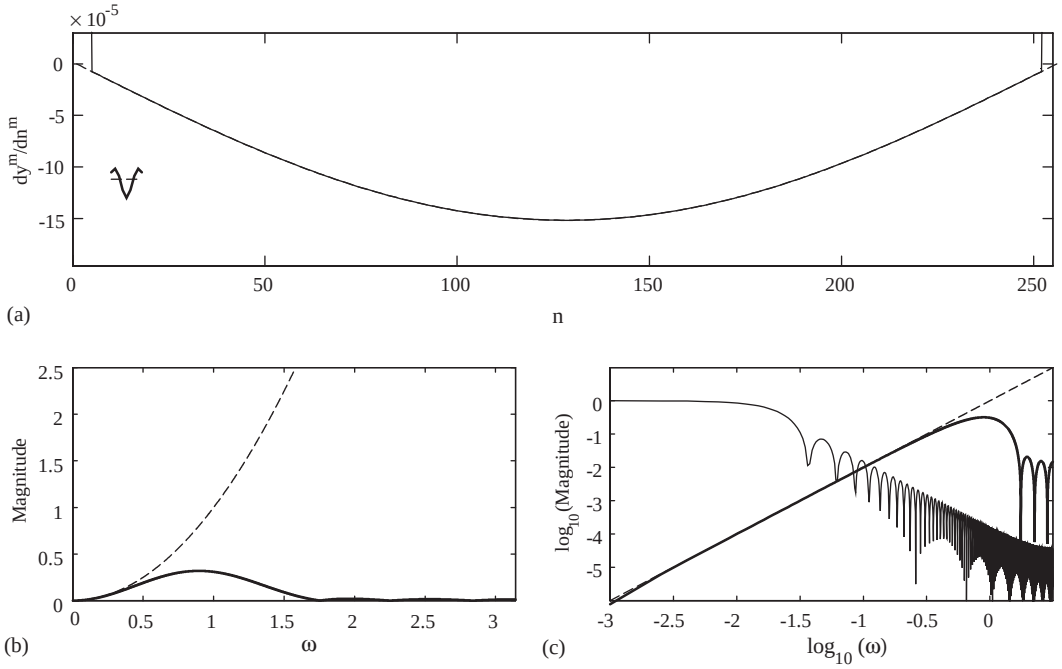

Fig. 6. Second derivative of the signal $y(n) = \sin(\pi n/(N-1))$ ($N = 256$) through a filter $h(n)_2$ ($N_f = 9$) designed by weighted least squares technique ($\omega_1 = 0.04$, $\omega_c = \pi/2$, $\alpha_1 = 1.0\mathrm{E}{+12}$, $\alpha_2 = 1.0$, $\beta = 1000.0$). Keys (a, b, c) referred to Fig. 4.

2.4. Lanczos's differentiator filters

It was well known (see Lanczos [20]) that a derivative, if simply considered as the limit of a finite difference, is of little value if sampled functions are not free from errors. For this reason, Lanczos resorted to a least squares method for solving the problem of first order differentiation of noisy data. In this regard, Lanczos obtained a very simple filter consisting of the following closed form:

$$h(n)_1 = \frac{3n}{2N_h^2 + 3N_h^2 + N_h}, \quad n = +N_h, \ldots, -N_h, \tag{19}$$

where N_h corresponds to half-length of the filter, being $N_f = 2N_h + 1$. Note that Eq. (19) has been reported here in its non-causal representation to be applied in a convolving operation (8). Lanczos obtained an equivalent form of Eq. (19) by fitting the assigned data through a local parabola and estimating the first derivative with an equivalent equation to Eq. (19). The concept can be generalized with higher order fitting polynomials to get higher order derivatives. However, filter (19) was considered by this author as a trade-off between computational efficiency and filtering performances when it was compared to the previous differentiator filters.

Fig. 7 illustrates the design of second order differentiator filters applied to the same discrete sequence ($y(n)$) used in the previous tests (Figs. 4–6). The designs, in the case of Lanczos's filter, were carried out only by changing (still heuristically) the number of points because Eq. (19) does not offer a direct access to the cutting frequency. This latter was observed through a visual

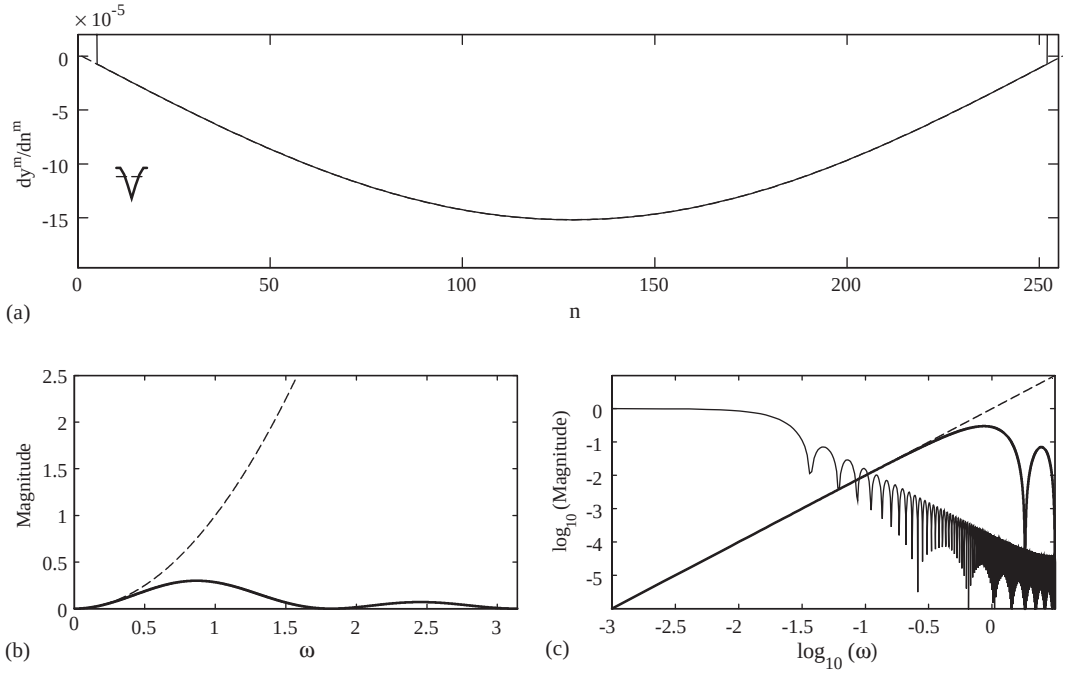

Fig. 7. Second derivative of the signal $y(n) = \sin(\pi n/(N-1))$ ($N = 256$) through a filter $h(n)_2$ ($N_f = 9$) obtained by cascading two first order differentiator filters ($h(n)_1$; $N_f = 5$) designed by Lanczos's method. Keys (a, b, c) referred to Fig. 4.

inspection of the transfer function. The comparison between Figs. 4, 5 and 6 respectively shows that the second order differentiator filters perform well.

3. Wavelet transforms as differentiator filters: the case of Gaussian wavelets (GW)

In this section the capability of certain continuous wavelet transforms for performing filtered differentiation is elucidated. This capability was partially observed through numerical tests by Gentile and Messina [19] within the framework of dynamical shapes corrupted by Gaussian noise. However, a theoretical correlation between the cwt_s and differentiator operators was not shown. Here this is made through the transformed Fourier domain.

A wavelet $\psi(x)$ is [18] a finite energy function having a zero average:

$$\int_{-\infty}^{+\infty} \psi(x)\,\mathrm{d}x = 0 \tag{20}$$

being $\psi(x)$ the *wavelet mother* from which the analyzing wavelets can be obtained by dilations (s: dilation parameter; $s \in \mathbb{R}^+$) and translations ($\bar{x}$: translation parameter; $\bar{x} \in \mathbb{R}$):

$$\psi(x)_{\bar{x},s} = \frac{1}{\sqrt{s}}\psi\left(\frac{x-\bar{x}}{s}\right) \tag{21}$$

by also weighting the *wavelet mother* with $s^{-1/2}$. The *wavelet mother* can be a real or complex function. However, in this context, apart from initial general considerations, real Gaussian wavelets are used. A continuous wavelet transform of a signal $y(x)$ corresponds to the following definition:

$$y(\bar{x})^w = \int_{-\infty}^{+\infty} y(x)\frac{1}{\sqrt{s}}\psi\left(\frac{x-\bar{x}}{s}\right)\mathrm{d}x. \tag{22}$$

The superscript w will distinguish the wavelet transform of $y(x)$ from the signal itself. Any capital letter will be used to indicate the relevant Fourier transform.

The wavelet transform (22) can be considered in the light of a convolution product (i.e., Eq. (4)) between the original signal $y(x)$ and the following convolving filter,

$$\psi(x;s) = \frac{1}{\sqrt{s}}\psi\left(-\frac{x}{s}\right) \tag{23}$$

which corresponds to the wavelet mother $\psi(x)$ dilated (through s), weighted (through $1/\sqrt{s}$) and turned over (through $-x$). Therefore, based on the classical Fourier transforms properties, Eq. (22) can be translated into

$$Y(\omega;s)^w = Y(\omega)\cdot\Psi(-s\omega)\sqrt{s}. \tag{24}$$

Eq. (24) corresponds to the Fourier transform of the signal filtered through $\Psi(-s\omega)\sqrt{s}$. A careful examination of the effect of this filter on the signal (i.e., through Eq. (24)) is worthy of attention.

Consider a wavelet mother $\psi(x)$ with a fast decay [18] that is defined by the mth derivative of a function $\theta(x)$ having a fast decay, using

$$\psi(x) = (-1)^m \frac{\mathrm{d}^m \theta(x)}{\mathrm{d}x^m}. \tag{25}$$

This is a sufficient and necessary condition establishing that the wavelet $\psi(x)$ is characterized by m vanishing moments [18]. Condition (26) also establishes that $\psi(x)$ has no more than m vanishing moments:

$$\int_{-\infty}^{+\infty} \theta(x)\,\mathrm{d}x = K \neq 0. \tag{26}$$

Therefore, based on the wavelets characterised by Eqs. (25,26), the following interesting equation can be proved:

$$\Psi(-s\omega)\sqrt{s} = s^{m+1/2}\Theta(-s\omega)(\mathrm{i}\omega)^m. \tag{27}$$

Indeed, if the Fourier transform of the dilated (through s), scaled (through $1/\sqrt{s}$) and turned over (through $-x$) version of Eq. (25) is considered:

$$\mathsf{F}\left(\psi\left(-\frac{x}{s}\right)\frac{1}{\sqrt{s}}\right) = \mathsf{F}\left(s^{m-1/2}\frac{\mathrm{d}^m\theta(-x/s)}{\mathrm{d}x^m}\right). \tag{28}$$

Eq. (3) together with the known properties of Fourier transforms leads to Eq. (27). A careful examination of Eq. (27) is now possible once the second term of Eq. (27) replaces the filter $\Psi(-s\,\omega)\sqrt{s}$ in Eq. (24). After this substitution is carried out, Eq. (24) transforms into

$$Y(\omega; s)^w = (\mathrm{i}\omega)^m Y(\omega) s^{m+1/2}\Theta(-s\omega). \tag{29}$$

Eq. (29) illustrates, in the Fourier transformed domain, that if the dilation parameter (s) is fixed to a certain value and $\Theta(-s\omega)$ is assumed to be a constant, then the wavelet transform of a signal ($y(x)$) would correspond to a proportional quantity of the mth derivative (with the wavelet mother having m vanishing moments). However, the function $\Theta(-s\omega)$ is far from being a constant. Its shape is the main reason for letting a wavelet transform correspond to a derivative or not. In particular, if $\Theta(-s\omega)$ behaved as a low pass filter, therefore having an approximately constant value in the pass band of interest, the wavelet transform (see Eq. (29)) would naturally correspond to a differentiator filter in the same band.

In general it is possible to prove that $\Theta(-s\omega)$ has similar characteristics to that of a low-pass filter. Firstly, condition (30) should be taken into account.

$$\Theta(\omega)_{\omega=0} = K = \int_{-\infty}^{+\infty} \theta(x)\,\mathrm{d}x \neq 0. \tag{30}$$

Moreover, it should also be considered that, because the behaviour of a wavelet is similar to that of a band pass filter, the magnitude $|\Psi(\omega)|$ is a function with fast decay. Consequently, based on the Fourier transform of Eq. (25) there is evidence that $|\Theta(\omega)|$ is also a function with a fast decay. Therefore, $|\Theta(\omega)|$ behaves as a function whose value at $\omega = 0$ is different from zero and tends to become negligible for $\omega \to \infty$.

Due to the fact that this study is involved in the use of Gaussian wavelets, it is interesting to focus attention on the characteristic curve of $\Theta(\omega)$ correspondent to the Gaussian wavelets.

A family of Gaussian wavelets can be obtained by applying Eq. (28) to the following modified Gaussian functions ($\theta(x)$) [19] which are based on a normal distribution having zero mean and unitary equivalent standard deviation:

$$\theta(x)_1 = -\mathrm{e}^{-x^2}\sqrt[4]{2/\pi}, \quad K_1 = -\sqrt[4]{2\pi}; \quad \theta(x)_2 = -\mathrm{e}^{-x^2}\frac{\sqrt[4]{2/\pi}}{\sqrt{3}}, \quad K_2 = -\frac{\sqrt[4]{2\pi}}{\sqrt{3}};$$

$$\theta(x)_3 = \mathrm{e}^{-x^2}\frac{\sqrt[4]{2/\pi}}{\sqrt{15}}; \quad K_3 = \frac{\sqrt[4]{2\pi}}{\sqrt{15}}; \quad \theta(x)_4 = \mathrm{e}^{-x^2}\frac{\sqrt[4]{2/\pi}}{\sqrt{105}}, \quad K_4 = \frac{\sqrt[4]{2\pi}}{\sqrt{105}} \tag{31}$$

to which the following Fourier transform corresponds:

$$\Theta(\omega)_m = K_m \mathrm{e}^{-\omega^2/4}. \tag{32}$$

Eq. (32) is obviously a low-pass filter (with zero-phase). Therefore, Eqs. (29,32) yield Eq. (33), which illustrates how the result of the convolution operated through Eq. (22) (i.e., wavelet transform) corresponds to a differentiation operated by a low-pass differentiator filter

$$\frac{Y(\omega;s)^w}{s^{m+1/2}K_m} = (\mathrm{i}\omega)^m \mathrm{e}^{-\omega^2 s^2/4} Y(\omega). \tag{33}$$

Obviously, it should be considered that this latter statement rigorously holds if the term of proportionality $K_m s^{m+1/2}$ is taken into account.

The maximum value of this low-pass differentiator filter in the transformed Fourier domain could conventionally correspond to the cutting frequency of the filter (ω_c). Based on Eq. (33) it becomes clear that such a maximum value can be evaluated by differentiating $\omega^m \mathrm{e}^{-(\omega s)^2/4}$ with respect to ω and by solving the equation equated to zero in ω. As a result, the expression of the cutting frequency can be evaluated in a closed analytical form as shown in the following:

$$\omega(s)_c = \sqrt{2m}/s, \tag{34}$$

where m still represents the order of differentiation of the mth Gaussian wavelet adopted (Gaus$m$).

Fig. 8 illustrates the differentiator filter ($|\Theta(s\omega)\omega^m|$) with different dilation parameters compared to the relevant ideal differential operator $|(\mathrm{i}\omega)^m|$. In particular Fig. 8b illustrates the excellent accuracy shown by the differentiator filter at lowest frequencies when the dilation parameter corresponds to $s = 6$. Fig. 8b undergoes the identical shifts of Fig. 3 for a greater clarity.

From Fig. 8 and the previous discussions the following conclusions can be drawn:

(i) To a certain extent Mallat's equation (35) can be generalized to the more practical context of differentiator filters where finite dilation parameters are of concern. The accuracy of the filter depends on the behaviour of the generating function ($\theta(x)$) in the Fourier transformed domain:

$$\lim_{s\to 0} \frac{y(x;s)^w}{s^{m+1/2}} = K_m \frac{\mathrm{d}^m y(x)}{\mathrm{d}x^m}. \tag{35}$$

(ii) The generating function ($\theta(x)$) of the mth Gaussian wavelet behaves as a linear low-pass filter. The dilation parameter can select the cutting frequency and the wavelet transform (22) naturally behaves as a low-pass differentiator filter.

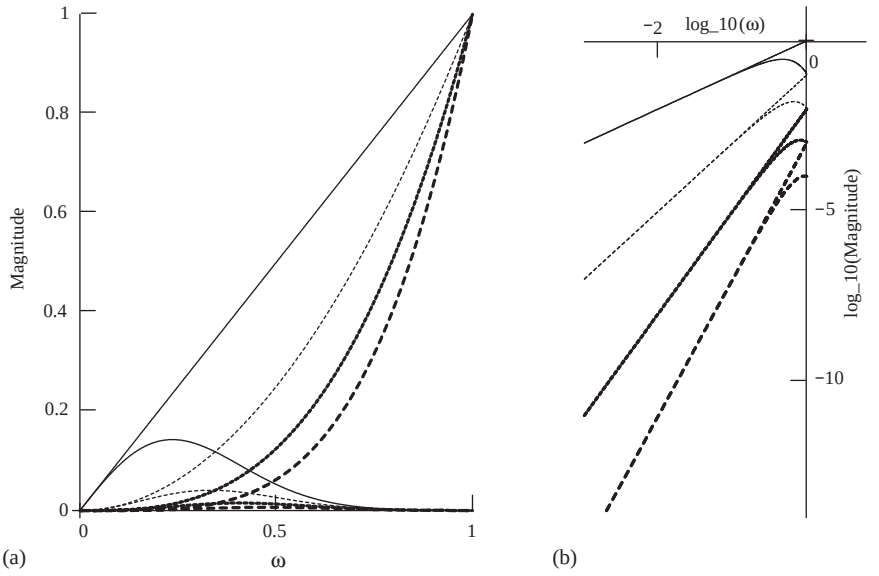

Fig. 8. Low-pass differentiator filters through continuous wavelet transforms based on Gaussian wavelets (for $m = 1, 2, 3, 4$: —, - - - -, ·····, - - - $|\Theta(s\omega)\omega^m|$ and ω^m, respectively; with $\omega_c = (2m)^{1/2}/s$ and $s = 6$).

(iii) The design of a digital low-pass differentiator filter can be avoided, at least in digital form, when a Gaussian wavelet transform is used. Indeed, only the passage from continuous to discrete sequences is required in order to make digital differentiator filters available.

3.1. Applying continuous wavelet transforms to discrete data

With respect to property (iii) Eqs. (23,33) are our main concern. The low-pass differentiator filter illustrated in Eq. (33) corresponds to the following impulse response function:

$$h(x)_m = \frac{1}{K_m s^{m+1/2}} \frac{\psi(-x/s)_m}{\sqrt{s}} \tag{36}$$

whose convolution on the signal $y(x)$ results in a low-pass filtered differentiation with a cutting frequency (ω_c) depending on the dilation parameter (s) through Eq. (34). The expressions of the related wavelets $\psi(x)$ that are used here can be found in Ref. [19] for $m = 1, 2, 3, 4$.

The passage from continuous signals to discrete ones follows the underlying theory illustrated in the previous Sections 2.1 and 2.2. However certain aspects need to be highlighted before applying cwt_s on discrete data.

In the frame of discrete signals the variable x (length) and the dilation parameter s will be substituted by n (samples) and a respectively thus yielding filters (37). This brings a certain generality to the sampled variable (space for dynamical shapes, etc.):

$$h(n)_m = \frac{1}{K_m a^{m+1/2}} \frac{\psi(-n/a)_m}{\sqrt{a}}. \tag{37}$$

A similar substitution can be made in Eq. (34) to obtain an analytical cutting frequency of Gausm wavelets depending on dilation parameter a. Moreover, although the Gaussian wavelets do not have a compact support here, for practical reasons, the support of the wavelet mother will be considered compact in $[-5, 5]$ for $m = 1, 2, 3, 4$.

The discrete filter represented in Eq. (37) has interesting differences compared to the filters illustrated in Section 2.

Through Gaussian cwt_s, the analyst must only settle the dilation parameter or equivalently, through Eq. (34), the cutting frequency. The number of sampling points depends on the dilation parameter as: $N_f = 10a + 1$. Table 1 lists both cutting frequency and length of filter (37) for several values of dilation parameter (a). An examination of Table 1 reveals how the higher that the dilation parameter is, the higher the length of the filter is, and the narrower the frequency pass band is.

In the FSW method cutting frequencies and number of points constitute two degrees of freedom for the design procedure. The design procedure of the WLS method is guided by six degrees of freedom $(\omega_1, \omega_c, \alpha_1, \alpha_2, \beta, N_f)$. Finally, Lanczos's filter has only the number of points as design parameters, because the cutting frequency depends on such a number of points.

Fig. 9 illustrates second order differentiator filters applied to the same discrete sequence ($y(n)$) used in the previous tests (Figs. 4–7). As has just been mentioned, this filter was not designed but it was directly applied (ready to use) after selecting a dilation parameter $a = 2$ to which the cutting frequency (Table 1) $\omega_c = 1$ corresponds. The comparison between Fig. 9 and previous relevant figures shows that filter (37) is extremely accurate even though no heuristic work was done to obtain it. Conversely, a number of trials is always needed in all methods mentioned in Section 2 in order to design appropriate FIR filters.

There is a minimum allowable value for the dilation parameter a that should be used with filter (37) when cwt_s are applied to discrete data. Such a limit is related to the shape of the Fourier

Table 1
Cutting frequencies, ω_c (Eq. (34)), corresponding to Gaussian wavelets with different vanishing moments m

a	m				Length (N_f)
	1	2	3	4	
1	1.41	2.00	2.45	2.83	11
2	0.707	1.00	1.22	1.41	21
3	0.471	0.667	0.816	0.943	31
4	0.354	0.500	0.612	0.707	41
5	0.283	0.400	0.490	0.566	51
6	0.236	0.333	0.408	0.471	61
7	0.202	0.286	0.350	0.404	71
8	0.177	0.250	0.306	0.354	81
9	0.157	0.222	0.272	0.314	91
10	0.141	0.200	0.245	0.283	101
11	0.129	0.182	0.223	0.257	111
12	0.118	0.167	0.204	0.236	121

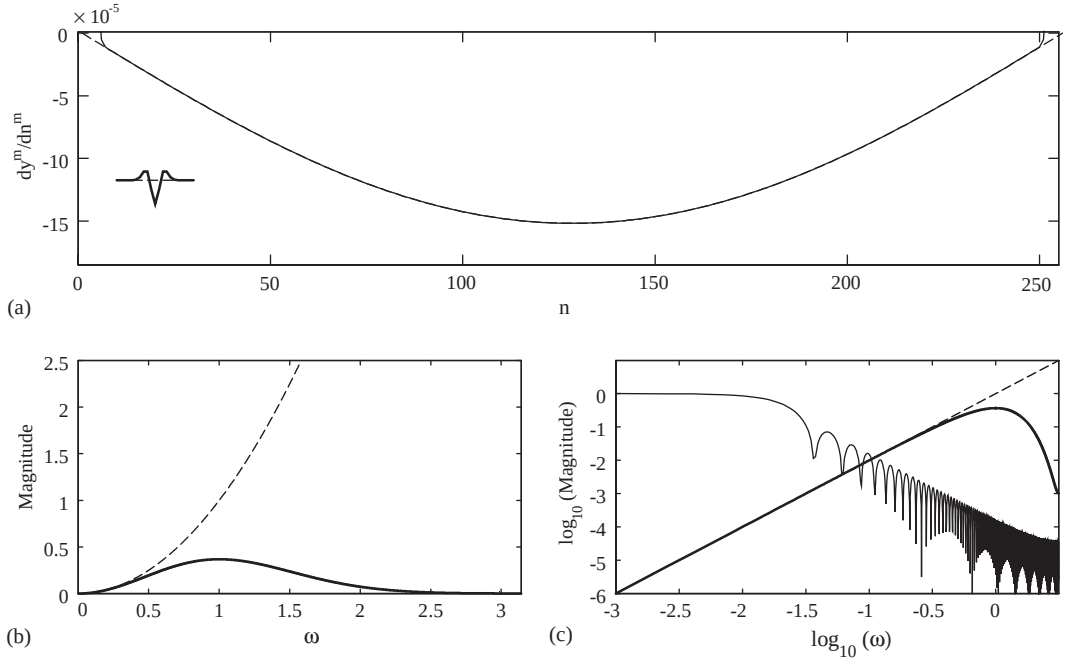

Fig. 9. Second derivative of the signal $y(n) = \sin(\pi n/(N-1))$ ($N = 256$) through a filter $h(n)_2$ ($N_f = 21$) based on wavelet Gaus2 ($\omega_c = 1.0$ and $a = 2$). Keys (a, b, c) referred to Fig. 4.

transform of $h(n)$ (i.e., $\bar{H}(\omega)$) in an inter-relationship with its analytical counterpart. This can be seen through Fig. 9. In particular, Fig. 9b shows a Fourier transform of the filter with a certain dropout, which cannot be directly designed by a parameter. As the dilation parameter decreases, cutting frequency increases (Eq. (34); Table 1) and the transfer function ($\bar{H}(\omega)$) approaches the maximum allowable threshold π. This trend can cause non-negligible *aliasing*, forcing the discrete transfer function (i.e., $\bar{H}(\omega)$) to deviate significantly from its theoretical counterpart ($H(\omega)$). A graphical examination of the discrete Fourier transforms of filters (37) can suggest that an $a_{min} = 2$ is reasonably prudent to reduce the aliasing of $\bar{H}(\omega)$ in the observable frequency band $[0, \pi]$ for $m = 1, 2, 3, 4$.

4. Identifying damage through cwt$_s$ and non-recursive differentiator filters

In this section the signal to be analyzed by digital differentiator filters and cwt$_s$ is obtained by sampling equally the displacements at discrete points of a transversally vibrating beam (Fig. 10). The same Fig. 10 illustrates the cracked beam that will be the main object of investigation here. The damaged vibrating beam is modelled as a segmented beam whose analytical model was presented in Ref. [11] and is referred to here as a classical Euler–Bernoulli beam model that neglects the rotatory inertia. The damage is simulated with an equivalent sub-beam which has a different Young's module. In particular, Young's module is obtained through Eq. (38) that was obtained through a slightly modified model presented by Bovsunovsky and Matveev [36], as

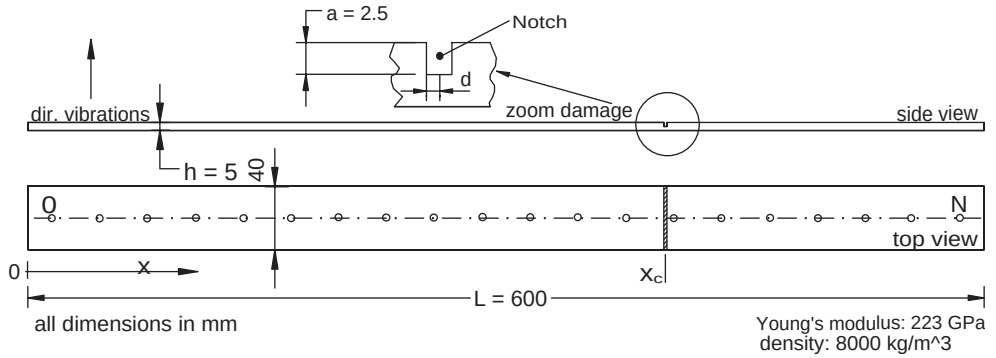

Fig. 10. Geometric, material characteristics and notations used for the beam model under investigation.

Table 2
First three natural frequencies (Hz) and percentage deviations for an undamaged and damaged FF-beam (refer to Fig. 16)

No.	Undamaged state	$\xi_c = 0.5$	dev%	$\xi_c = 0.667$	dev%	$\xi_c = 0.85$	dev%
1	75.38	72.58	3.7	73.64	2.3	75.20	0.24
2	207.8	207.8	0.0	201.7	2.9	205.4	1.2
3	407.3	396.1	2.7	406.4	0.22	397.4	2.4

reported in Gentile and Messina [11]:

$$\frac{E_{eq}}{E} = \left[(1-\gamma)^3 + \frac{4.41}{12}\frac{(1-\gamma)}{d/h}[(1-\gamma)^6 - 3(1-\gamma)^2 + 2]\right]^{-1}. \tag{38}$$

Based on Fig. 10, γ corresponds to the ratio $a/h = 0.5$ and d is representative of the halfwidth of the notch ($d = 1$ mm). The analytical model simulates the notch as symmetrically placed around the barycentric axis of the undamaged beam and located at the coordinate x_c.

As far as the simulated damaged scenario is concerned Table 2 has been taken into account.

Mode shapes in damaged and undamaged conditions are not shown for brevity's sake. Here it is recalled that several authors have shown how a visual inspection of the mentioned dynamical shape does not clearly indicate the place of local damage (e.g., Refs. [4,5,11]). This justifies the need to resort to opportune processing of discrete data that make the damage evident through significant peaks located on smooth dynamical shapes.

Any simulation regarding uncontaminated data will not be considered. Indeed, the previous sections and the previous investigations [4,5,11,19] clearly illustrate that differentiator filters and cwt_s are certainly and efficiently able to locate local damage through the digital processing of clean data.

4.1. Data contaminated by Gaussian noise

This section illustrates the potential of cwt_s and digital differentiator filters when applied to discrete data contaminated by noise. In the following simulations the noise has been simulated by

adding a Gaussian noise $n(x)$ to the true signal $y(x)_t$:

$$y(x) = y(x)_t + n(x)_{\mu,\sigma} \tag{39}$$

μ and σ being the mean and the standard deviation of the normal distribution respectively. The parameters (μ, σ) adopted in the simulations have been chosen by following Ref. [19]. In particular, for comparison purposes an identical *seed* generating the random sequence simulating the Gaussian noise was retained.

Fig. 11 reports the processing of the first mode shape of an FF damaged beam (refer to Fig. 10, Table 2) through different filters (depicted in each relevant graph). Fig. 11(a) illustrates the performance obtained by Gaus2 cwt_s (second derivative) which has a dilation parameter $a = 9$. This latter condition establishes a filter having $N_f = 91$ points $(10a + 1)$ with a cutting frequency $\omega_c = 0.22$. Therefore, the remaining filters were designed in order to have a cutting frequency (ω_c) approximately equal to 0.2 and a minimum number of points that were able to preserve the accuracy of the design and reduce the loss of data at the ends. In the case of Lanczos's filter the minimum number of points coincides with the number of points that ensures a cutting frequency of 0.2.

All the designs of the differentiator filters were carried out by trial and error through changing the designing parameters that are summarized in Table 3 for each filter. The quality of the design was checked by a visual inspection of the relevant $\bar{H}(\omega)$ in both linear and logarithmic scales.

The FSW method was not able to identify an accurate second order differentiator filter $(m = 2)$ by a $\omega_c = 0.2$ and $N_f = 91$ points due to the inaccuracies at low frequencies. However, it was possible to design a filter $h(n)_2$ by cascading a first order $(h(n)_1)$ differentiator filter. The cascading procedure provided an $h(n)_2$ with a ω_c (meant as the maximum of $\bar{H}(\omega)$) close to 0.2 and $N_f = 81$ points. Apart from a clear equivalence that Fig. 11 shows between this filter and the filter obtained through the GW method, a significantly better performance cannot be clearly detected. It is interesting to observe the similarity between the convolving filter regarding the FSW method and the filter corresponding to the GW method.

The design of Lanczos's filter, obtained by cascading one first order differentiator filter, was straightforward. Only 45 points were able to provide a ω_c at about 0.18 with a performance clearly comparable with previously mentioned filters. Again, the filter was obtained by cascading two first order differentiator filters.

The design through the WLS method was felt to be the most laborious one. After selecting the six parameters needed (Table 3) the filter consisted of 46 points with a ω_c established at 0.2. The loss of data at the ends, similarly to Lanczos's filter, was slightly worse than that of the GW and FSW method.

It should be said that the design procedures for all the mentioned filters (excluding wavelet based filters) showed an increasing difficulty when lower cutting frequencies were required. Conversely the cwt based on Gaussian wavelets does not undergo an appreciable difference for any order of differentiation $(m = 1, 2, 3, 4)$ at lower cutting frequencies (higher dilation parameter a). On the other hand, the FIR filters discussed here (FSW, WLS, L) and others available in the literature have the advantage that they can be designed as full band or *quasi*-full band differentiators, whilst the cwt_s based on Gaussian wavelets undergo a higher limit in the observable frequency band because of the minimum allowable value of the dilation parameter discussed in Section 3.

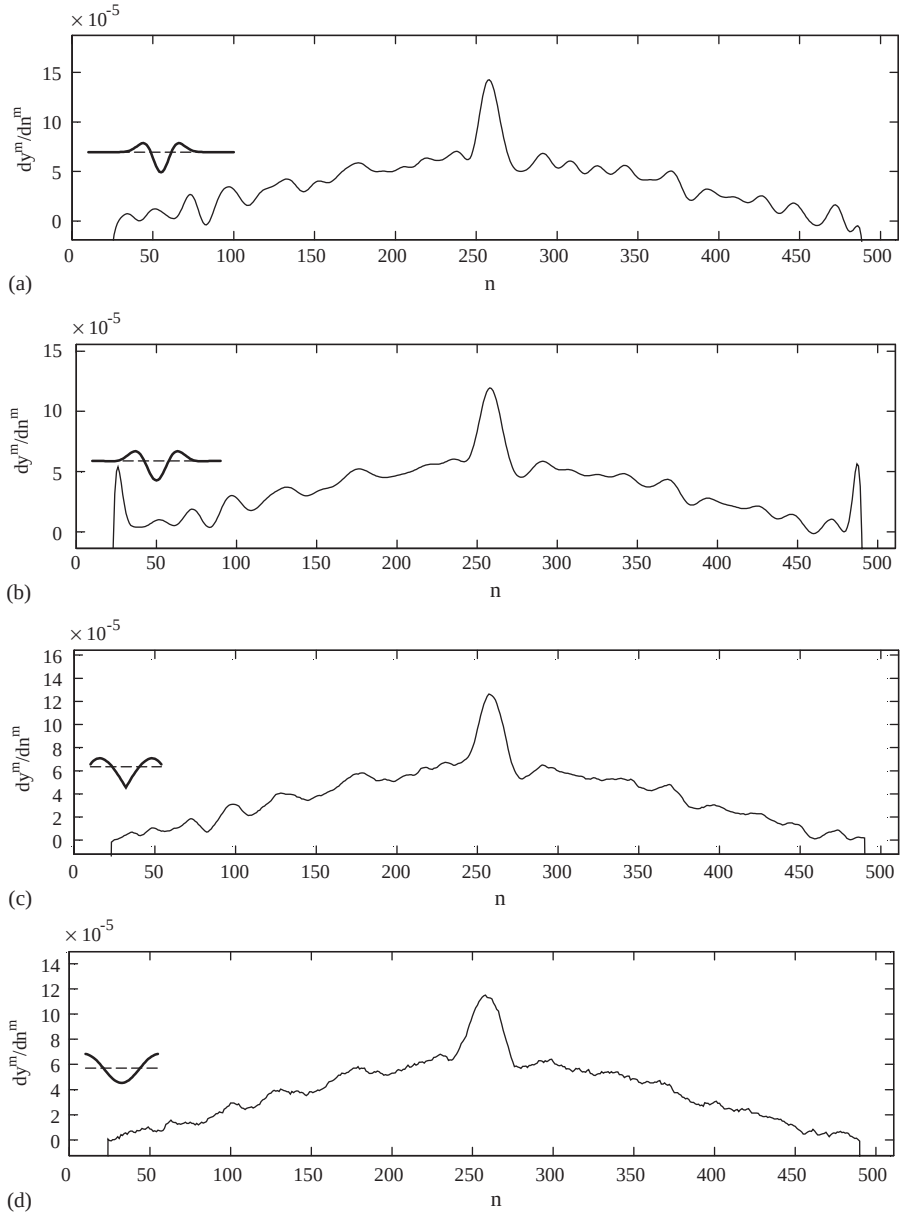

Fig. 11. Processing of the first mode shape of an FF damaged beam (refer to Fig. 10) through different filters. Noise added to the mode shape: Gaussian, $\mu = 0$, $\sigma = 0.2\%$ of the maximum amplitude of the mode shape. Crack at $\xi_c = x_c/L = 0.5$ (refer to Table 2); $N = 512$. [(a) GW, Gaus2, $\omega_c = (2m)^{1/2}/a$, $a = 9$, $N_f = 91$; (b) FSW, by $h(n)_1 * h(n)_1$, $\omega_c = 0.2$, $N_f = 81$; (c) L, by $h(n)_1 * h(n)_1$, $\omega_c = 0.18$ and $N_f = 45$; (d) WLS, by $h(n)_2$, $\omega_1 = 0.02$, $\omega_c = 0.2$, $\alpha_1 = 1.0\text{E}+10$, $\alpha_2 = 1.0$, $\beta = 100.0$, $N_f = 46$].

Figs. 12 and 13 illustrate a comparison similar to that shown in Fig. 11; the notch is located at $x_c/L = 0.667$ and 0.85 respectively. In both of the figures the most sensitive modes are analyzed. Those modes were selected through the relative changes of the respective natural frequencies listed

Table 3
Designing parameters of the discussed FIR differentiator filters

No.	Name	Acronym	Designing parameters
1	Fourier series and windows	FSW[a]	N_f, ω_c
2	Weighted least squares	WLS	N_f, ω_c, ω_1, α_1, α_2, β
3	Lanczos	L	N_f
4	cwt_s through Gaussian wavelets	GW	a

[a] Based on Hamming's window.

in Table 2. As is clear from Figs. 12 and 13 similar conclusions to those from Fig. 11 can be drawn.

In addition, a global examination of Figs. 11–13 would suggest that the differentiator filters based on the FSW, L, WLS methods are able to realize a differentiation which is smoother than the GW method in the region where there is no damage. This has to be considered an advantage because it makes the identification of abnormal peaks (damage) clearer. However, it should also be considered that the cutting frequencies mentioned in all the methods discussed are not equivalent, as well as taking into account that the GW method used a slightly higher cutting frequency than that adopted for the other methods. This latter observation can be observed in Fig. 14 where the GW method was implemented by using higher dilation parameters that performed better in terms of smoothness but showing a slightly increasing boundary effect.

5. Conclusion

A theoretical and numerical solution for certain mathematical tools (cwt_s) has been presented dealing with the identification of local damage occurring in transversally vibrating (or statically deformed) beams. Numerical simulations accounting for free or noisy data have also supported such a theoretical solution.

It has been theoretically shown how certain continuous wavelet transforms applied to discrete data can consist of particular differentiator FIR filters.

Several FIR differentiator filters have been adopted in this study for a comparison with cwt_s. Such differentiator filters have been chosen in an attempt to represent the technical proposals suggested over the last 20 years in the area of digital signal processing. However, this attempt should not be considered a review of all the existing digital differentiator filters. Rather, this investigation has been carried out to clarify the difference between cwt_s, based on Gaussian wavelets, compared to existing techniques.

Gaussian based cwt_s can be considered superior to the adopted non-recursive differentiator filters in terms of *simplicity*. Indeed, the theoretical part has showed how the analyzed cwt_s do not require any design because they are naturally compact differentiator filters. Conversely, the analyzed filters needed a non-negligible amount of heuristic work to be appropriately designed. Only the simplicity of Lanczos's filter has been felt to be comparable to the simplicity of the cwt_s.

The simulations have also shown that in certain circumstances the differentiator filters can offer a valid alternative *in terms of efficiency and length*.

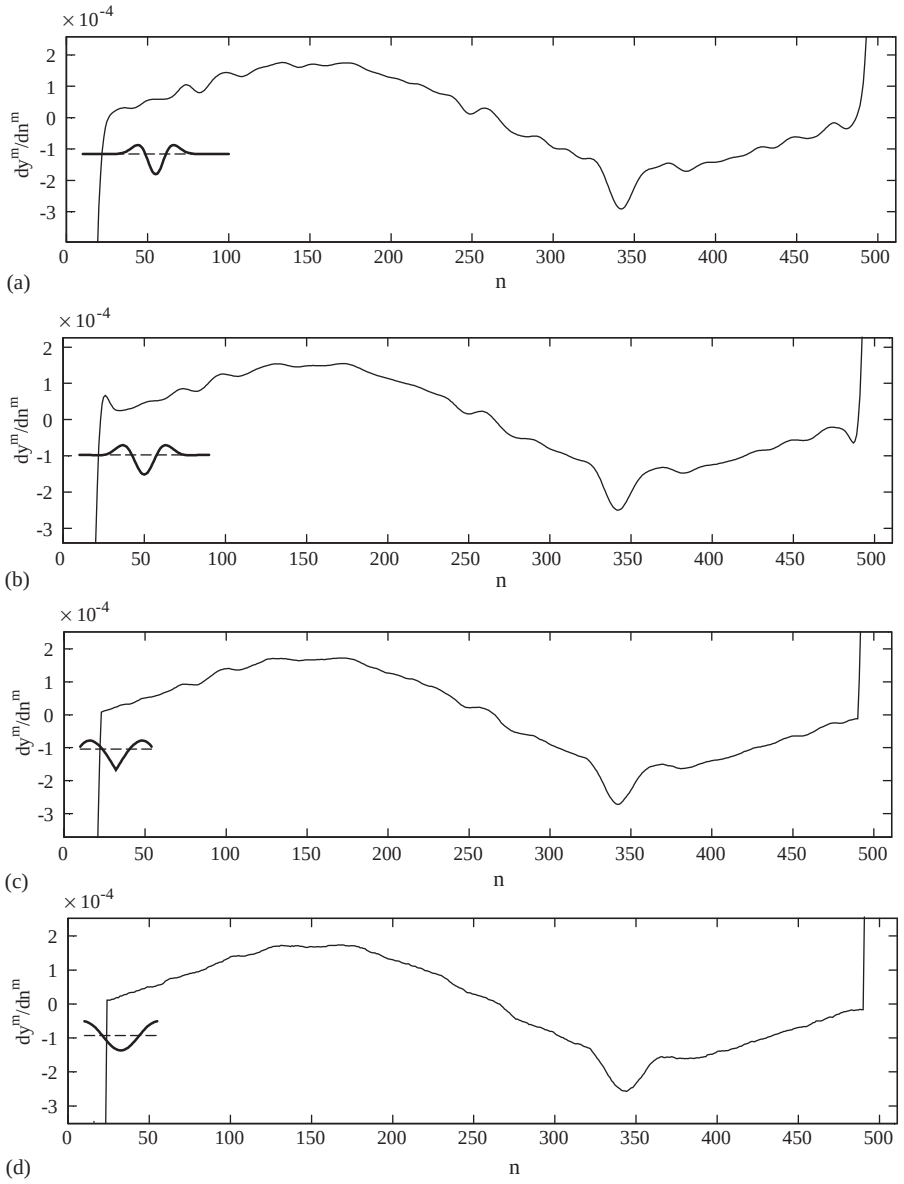

Fig. 12. Processing of the second mode shape of an FF damaged beam (refer to Fig. 10) through different filters. Noise added to the mode shape: Gaussian, $\mu = 0$, $\sigma = 0.2\%$ of the maximum amplitude of the mode shape. Crack at $\xi_c = x_c/L = 0.667$ (refer to Table 2); $N = 512$. Keys (a, b, c, d) referred to Fig. 11.

In any case the present study has shown that derivatives and cwt_s have very similar performance and cannot be considered two distinguished and completely different mathematical tools.

Further questions remain to be explained especially within the framework of the existing wavelets that could be adopted to identify local damage by processing dynamical shapes.

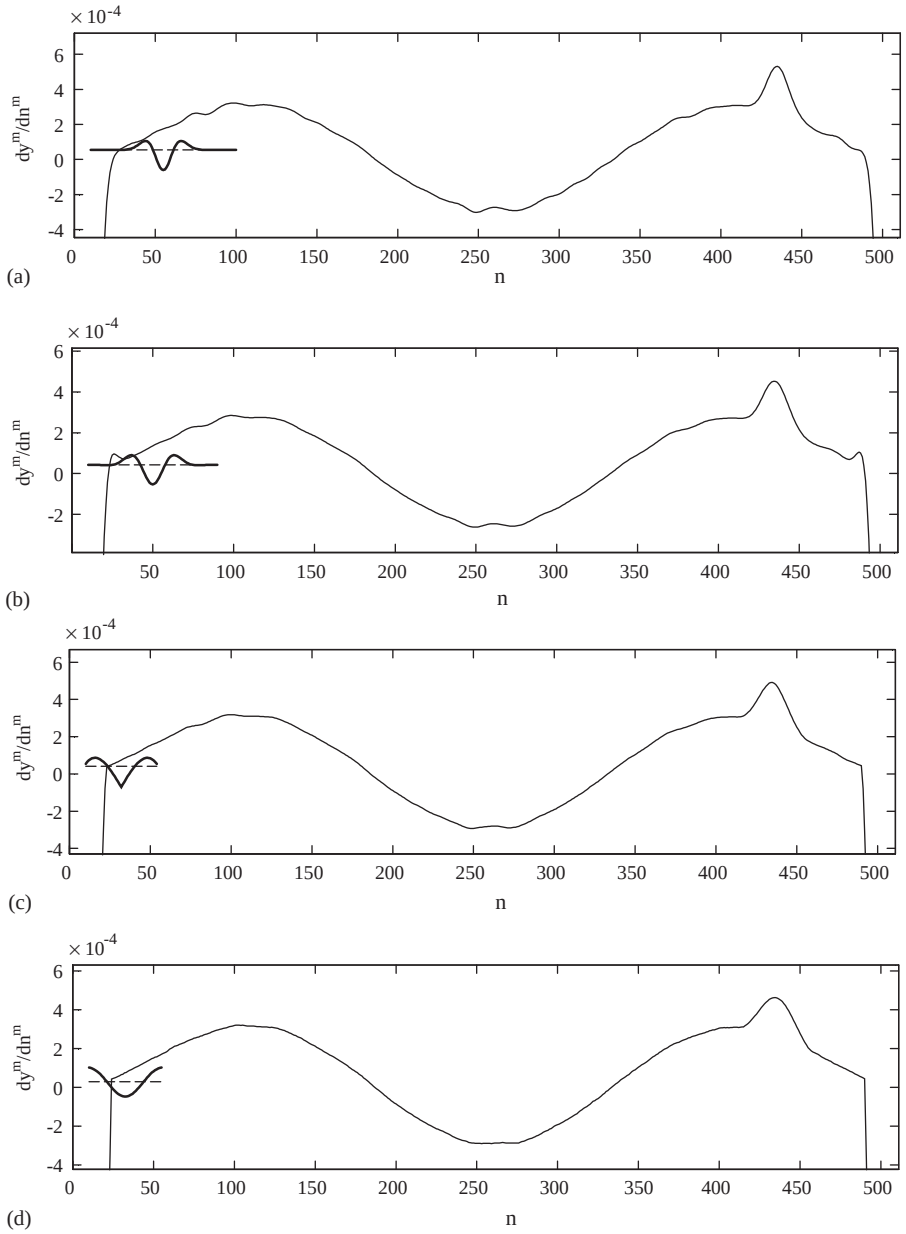

Fig. 13. Processing of the third mode shape of an FF damaged beam (refer to Fig. 10) through different filters. Noise added to the mode shape: Gaussian, $\mu = 0$, $\sigma = 0.2\%$ of the maximum amplitude of the mode shape. Crack at $\xi_c = x_c/L = 0.85$ (refer to Table 2); $N = 512$. Keys (a, b, c, d) referred to Fig. 11.

Finally, apart from the valuable theoretical solutions and numerical comparisons made, this work constitutes, in its relevant field, the first attempt to process derivatives in order to identify local damage by taking into account a processing technique aimed at reducing the instability of derivatives of noisy data.

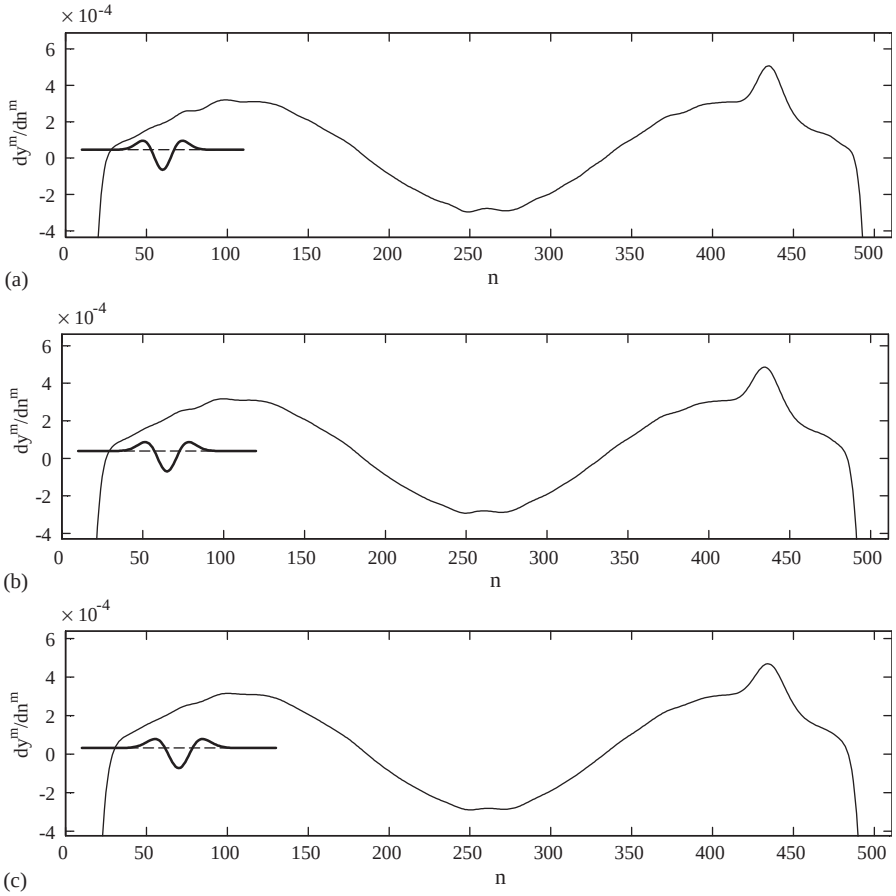

Fig. 14. Processing of the third mode shape of an FF damaged beam (refer to Fig. 13) through cwt_s having different dilation parameters ((a, b, c): $a = 10, 11, 12$ respectively).

Acknowledgements

The Library of the DEE (Dipartimento di Elettrotecnica ed Elettronica) of Politecnico di Bari (Italy) is acknowledged for the assistance provided during the preparation of this manuscript. Prof. Mollova from Department of Computer-Aided Design, UACEG-Sofia (Bulgaria) is also acknowledged for having promptly made available Refs. [34,35]. Finally, the author wishes to thank the Editor for the accurate editing of the manuscript.

This work was partially supported by the basic research funds (ex-60%) awarded to the author in 2002.

References

[1] A.D. Dimarogonas, Vibration of cracked structures: a state of the art review, *Engineering Fracture Mechanics* 55 (5) (1996) 831–857.

[2] O.S. Salawu, Detection of structural damage through changes in frequency: a review, *Engineering Structures* 19 (9) (1997) 718–723.
[3] S.W. Doebling, C.R. Farrar, M.B. Prime, A summary review of vibration-based damage identification methods, *The Shock and Vibration Digest* 30 (2) (1998) 91–105.
[4] M.M.F. Yuen, A numerical study of the eigenparameters of a damaged cantilever, *Journal of Sound and Vibration* 103 (3) (1985) 301–310.
[5] A.K. Pandey, M. Biswas, M.M. Samman, Damage detection from changes in curvature mode shapes, *Journal of Sound and Vibration* 145 (2) (1991) 321–332.
[6] M.A.-B. Abdo, M. Hori, A numerical study of structural damage detection using changes in the rotation of mode shapes, *Journal of Sound and Vibration* 251 (2) (2002) 227–239.
[7] J. Chance, G.R. Thomlinson, K. Worden, A simplified approach to the numerical and experimental modelling of the dynamics of a cracked beam, *Proceedings of the* 12*th International Modal Analysis Conference*, Honolulu, HI, 1994, pp. 778–785.
[8] D.V. Jauregui, C.R. Farrar, Comparison of damage identification algorithms on experimental modal data from a bridge, *Proceedings of the* 14*th International Modal Analysis Conference*, 1996, pp. 1423–1429.
[9] B.C. Hoerst, C.P. Ratcliffe, Damage detection in beams using laplacian operators on experimental modal data, *Proceedings of the* 15*th International Modal Analysis Conference*, Orlando, FL, 1997, pp. 1305–1311.
[10] C.P. Ratcliffe, W.J. Bagaria, Vibration technique for locating delamination in a composite beam, *American Institute of Aeronautics and Astronautics Journal* 36 (6) (1998) 1074–1077.
[11] A. Gentile, A. Messina, Detection of cracks by only measured mode shapes in damaged conditions, *Proceedings of the Third International Conference on Identification in Engineering Systems*, Swansea, Wales, UK, 2002.
[12] Q. Wang, X. Deng, Damage detection with spatial wavelets, *International Journal of Solids and Structures* 36 (1999) 3443–3468.
[13] S.T. Quek, Q. Wang, L. Zhang, K.K. Ang, Sensitivity analysis of crack detection in beams by wavelet technique, *International Journal of Mechanical Sciences* 43 (2001) 2899–2910.
[14] J.C. Hong, Y.Y. Kim, H.C. Lee, Y.W. Lee, Damage detection using the Lipschitz exponent estimated by the wavelet transform: applications to vibration modes of a beam, *International Journal of Solids and Structures* 39 (2002) 1803–1816.
[15] A. Haar, Zur theorie der orthogonalen funktionensysteme, *Mathematische Annalen* 69 (1910) 331–371.
[16] I. Daubechies, *Ten Lectures on Wavelets*, SIAM, Philadelphia, PA, 1992.
[17] M. Holschneider, *Wavelets an Analysis Tool*, Clarendon Press, Oxford, 1995.
[18] S. Mallat, *A Wavelet Tour of Signal Processing*, Academic Press, New York, 2001.
[19] A. Gentile, A. Messina, On the continuous wavelet transforms applied to discrete vibrational data for detecting open cracks in damaged beams, *International Journal of Solids and Structures* 40 (2003) 295–315.
[20] C. Lanczos, *Applied Analysis*, Dover, New York, 1988.
[21] A.V. Oppenheim, R.W. Schafer, *Digital Signal Processing*, Prentice-Hall, Englewood Cliffs, NJ, 1975.
[22] L.R. Rabiner, B. Gold, *Theory and Application of Digital Signal Processing*, Prentice-Hall, Englewood Cliffs, NJ, 1975.
[23] K.R. Otnes, L. Enochson, *Applied Time Series Analysis*, Vol. I, Wiley, New York, 1978.
[24] A. Papoulis, *The Fourier Integrals and its Applications*, McGraw-Hill, New York, 1984.
[25] H. Dym, H.P. McKean, *Fourier Series and Integrals*, Academic Press, New York, 1972.
[26] D.J. Ewins, *Modal Testing: Theory and Practice*, Wiley, New York, 1992.
[27] C.A. Rahenkamp, B.V.K. Kumar, Modifications to the McClellan, Parks and Rabiner computer program for designing higher order differentiating FIR filters, *IEEE Transactions on Acoustics, Speech, and Signal Processing* ASSP-34 (6) (1986) 1671–1674.
[28] J.H. McClellan, T.W. Parks, L.R. Rabiner, A computer program for designing optimum FIR linear phase digital filters, *IEEE Transactions on Audio Electroacoustics* AU21 (1973) 506–526.
[29] S.C. Pei, J.J. Shyu, Eigenfilter design of higher-order digital differentiators, *IEEE Transactions on Acoustics, Speech, and Signal Processing* 37 (4) (1989) 505–511.
[30] S.C. Pei, J.J. Shyu, Analytic closed-form matrix for designing higher order digital differentiators using eigen-approach, *IEEE Transactions on Signal Processing* 44 (3) (1996) 698–701.

[31] M.R.R. Reddy, B. Kumar, S.C. Dutta Roy, Design of efficient second and higher order FIR digital differentiators for low frequencies, *Signal Processing* 20 (1990) 219–225.
[32] H. Shah, S.C. Dutta Roy, B. Kumar, On the design of efficient second and higher degree FIR digital differentiators at the frequency π/(any integer), *Signal Processing* 27 (1992) 117–124.
[33] S. Sunder, R.P. Ramachandran, Least-squares design of higher order nonrecursive differentiators, *IEEE Transactions on Signal Processing* 42 (4) (1994) 956–961.
[34] G. Mollova, Compact formulas for least-squares design of digital differentiators, *Electronics Letters* 35 (20) (1999) 1695–1697.
[35] G. Mollova, R. Unbehauen, Analytical design of higher-order differentiators using least squares technique, *Electronics Letters* 37 (17) (2001) 1098–1099.
[36] A.P. Bovsunovsky, V.V. Matveev, Analytical approach to the determination of dynamic characteristics of a beam with a closing crack, *Journal of Sound and Vibration* 235 (3) (2000) 415–434.